20111021A

厚生労働科学研究費補助金
医療機器開発推進研究事業

循環腫瘍細胞観察可能なナノ粒子質量顕微鏡開発に関する研究

平成23年度　総括研究報告書

研究代表者　瀬藤　光利

平成24（2012）年4月

目　　次

厚生労働科学研究費補助金（医療機器開発推進研究事業）　総括研究報告書

循環腫瘍細胞観察可能なナノ粒子質量顕微鏡開発に関する研究

研究代表者　浜松医科大学・解剖学講座・細胞生物学分野　教授　瀬藤光利

研究要旨

癌が進展するごく早期から血中に存在する循環腫瘍細胞の質的評価は診断・治療に重要である。本研究は、研究代表者が開発した質量顕微鏡装置を用いて循環腫瘍細胞の質的評価を行うことを目的とする。本事業年度は、大腸癌及び乳癌細胞株を用い循環腫瘍細胞を精製・回収するための手法を最適化し、一細胞レベルでのナノ粒子質量顕微鏡法解析を行った。大腸癌と乳癌の担癌患者末梢血から循環腫瘍細胞を精製し質量顕微鏡解析することにより、循環腫瘍細胞の質的評価系を確立した。

研究分担者氏名・所属研究機関名及び所属研究機関における職名

瀬藤光利　浜松医科大学・解剖学講座・細胞生物学分野　教授

池上浩司　浜松医科大学・解剖学講座・細胞生物学分野　准教授

早坂孝宏　浜松医科大学・解剖学講座・細胞生物学分野　特任助教

A．研究目的

厚生労働行政において癌対策及び癌研究の推進は重要な位置を占める。癌の早期診断、予後判定、治療効果判定はいずれも重要な課題であり、その方法が種々議論され開発されてきた。転移に関する分子メカニズムの解明は、これらいずれの課題にも極めて重要な解決の糸口となりうるテーマである。転移に関して提唱され注目を集めている新規モデルは、従来考えられてきたよりもごく早い病期のうちから、癌細胞が血液中に流れ出し、やがて多臓器に生着し転移巣を形成するというものである。この血液中に存在する腫瘍細胞は循環腫瘍細胞と呼ばれ、検出個数と予後の悪さには正の相関関係があることが知られている。一方で循環腫瘍細胞の質的な評価に関しては細胞表面マーカーや遺伝子発現に着目した報告が行われているのみであり、評価方法は未だ十分に確立されていない。本研究はこの評価方法を提唱するために循環腫瘍細胞の収集と解析を行うことを目的とする。

本研究では、質量顕微鏡法による腫瘍組織および循環腫瘍細胞の解析を行い、その生物学的特性を明らかにして腫瘍細胞機能イメージング新評価システムを確立し、病理検査に応用する。質量顕微鏡法は研究代表者らが開発してきた質量分析手法であり、生体試料を直接的に二次元質量分析することにより、試料組織上生体物質の種類、位置、相対量を解析する手法である。本研究では、新たな循環腫瘍細胞の質的評価方法の確立を目指すために、担癌患者検体から循環腫瘍細胞を回収しナノ粒子質量顕微鏡法による統合的解析を行うことを目的とする。末梢血および参照試料としての原発巣組織の採取対象として大腸癌・乳癌を設定した。大腸癌は労働年齢に好発し、乳癌は女性特有の癌であるから、厚生労働行政の目指す「働く世代のがん対策」及び「女性特有のがん対策の推進」に貢献すると考えられる。

本事業年度は、少数の循環腫瘍細胞を回収し質量顕微鏡観察することを可能とするために、1）担癌患者検体の収集、2）担癌患者より採取した末梢血から循環腫瘍細胞を回収する手法の最適化、3）一細胞ナノ粒子質量顕微鏡解析法の最適化、4）臨床検体の一細胞質量顕微鏡解析を行った。

B．研究方法

1）臨床検体の取得にあたっては、浜松医科大学消化器外科で診断もしくは治療を目的として組織採取を行う大腸癌及び乳癌患者を対象とした。十分なインフォームドコンセントを行い同意の得られた患者から、生検組織採取とともに循環腫瘍細胞採取のため末梢血の採血を行った。上記対象患者を研究協力者の所属施設で収集し、収集試料は連結可能匿名化し、研究代表者施設管理者が管理した。

2）循環腫瘍細胞の選択の基本手法としては、全体計画の通り磁気細胞分離法とフローサイトメトリー法を利用した。正常人血液に細胞株を添加し作製するモデル血液での実験には、大腸癌細胞株 HCT116 及び乳癌細胞株 SKBR-3 を培養し用いた。蛍光標識化合物、バッファ、遠心管につき最適化を行った。

3）フローサイトメトリー法により精製された細胞の回収及び接着条件を、接着・洗浄後の細胞回収率に基づき比較検討した。スライドグラスのコーティング剤の比較も行った。検討結果をもとに ITO ナノ粒子成膜スライドグラスへの接着性検討を行った。質量顕微鏡解析の条件としてレーザーエネルギー、空間解像度、測定領域範囲、測定質

量範囲等を最適化した。
4) 原発巣の単一細胞化には、研究全体計画時に考案した通り、検体組織をメスで小断片化した後に酵素処理する方法を用いた。フローサイトメトリー法により細胞を回収し、一細胞質量顕微鏡解析した。
（倫理面への配慮）
本研究は浜松医科大学の医の倫理審査委員会による承認を受けた。該当する患者に当研究に関して患者用説明文書を用い、研究への協力の可否が治療の質に影響しないこと、研究への協力が危険を伴わないこと、研究協力者及び家族の意思を第一に尊重することを十分に説明し、インフォームドコンセントを得られたた場合、文書による同意書を得て、疫学研究に関する倫理指針（平成１６年文部科学省・厚生労働省告示第２号）および臨床研究に関する倫理指針（平成１６年厚生労働省告示第４５９号）に厳正に則り研究を施行した。試料は連結可能匿名化を行い情報管理者が適切に管理した。

C．研究結果
1) 初年度から検体の収集を行うとした全体研究計画の通り、大腸癌・乳癌臨床検体につき末梢血の収集と循環腫瘍細胞の精製・解析を行った。
2) 大腸癌及び乳癌細胞株を用い循環腫瘍細胞の精製条件を最適化した。抗体、バッファ、遠心管の最適化により高いコントラストで循環腫瘍細胞を分離することができるようになった。
3) 精製された循環腫瘍細胞の回収・接着方法を比較検討することで、細胞回収率を向上することができた。最適な細胞接着をもたらすコーティング条件を用いたナノ粒子成膜処理したスライドグラスへの循環腫瘍細胞の接着・回収に成功した。一細胞質量顕微鏡法の解析条件を検討し、細胞が接着した領域に高いシグナル強度で検出される分子を見出すことができた。
4) 原発巣検体試料に由来する細胞の質量顕微鏡法解析により、細胞接着部位に検出される分子が見出された。大腸癌・乳癌患者末梢血からの循環腫瘍細胞取得方法を最適化し、乳癌循環腫瘍細胞を精製し質量顕微鏡解析し、細胞の接着した部位に高いシグナル強度で検出される分子を見出した。ナノ粒子で成膜処理したスライドグラス上に原発巣由来細胞及び循環腫瘍細胞を接着し一細胞質量顕微鏡解析を行った。

D．考察
1) 症例の収集に際し臨床医と連携することで、予定通りのペースで検体の回収が達成できた。症例情報と解析結果の統合的検討により新たな予後因子や治療効果判定の発見に寄与する研究成果を取得することが今後期待される。
2) 循環腫瘍細胞は極めて少数であり、本研究開始当初は精製の過程で失われることが多かった。循環腫瘍細胞選択手法の条件最適化を行った結果、安定して循環腫瘍細胞を検出し回収することが可能となった。
3) 細胞回収・接着手法の最適化により、一細胞質量顕微鏡法解析に適した条件が確立された。高解像度質量顕微鏡の発展型として本講座が島津製作所と共同開発した質量顕微鏡装置（Mass Microscope）は、光学顕微鏡を装置中に導入することにより、可視光顕微鏡像とシグナル強度マップを高い精度で対応づけ分子分布を解析することを可能とした。一細胞を対象とした超微小領域での質量顕微鏡法解析に成功したのはこの装置の利用によるところが大きいと考える。
4) 循環腫瘍細胞の性状解析に関する研究では、免疫染色による検討や限られた遺伝子数でのマイクロアレイの報告があるが、質量顕微鏡法を用いた解析については未だ報告がない。本研究では、臨床検体を用いた質量顕微鏡解析において検出された分子群に着目し、循環腫瘍細胞の性状評価手法を確立したい。

E．結論
大腸癌と乳癌の循環腫瘍細胞の精製・回収手法を確立し、臨床検体を用いた循環腫瘍細胞の回収と質量顕微鏡法解析を行い、細胞特異的に検出される分子群を見出した。ナノ粒子を利用した一細胞質量顕微鏡法解析手法の最適化を行った。一細胞質量顕微鏡法により単一細胞レベルの分子分布を可視化するための手法を確立した。

F．健康危険情報
本事業年度は特に健康危険情報は報告すべきものはなかった。

G．研究発表
1. 論文発表
【原著論文】
(1) Yamada M, Yao I, Hayasaka T, Ushijima M, Matsuura M, Takada H, Shikata N, Setou M, Kwon KH, Ito S. Identification of oligosaccharides from histopathological sections by MALDI imaging mass spectrometry. Anal Bioanal Chem. 2012 Feb;402(5):1921-30.
(2) Tanaka H, Zaima N, Sasaki T, Yamamoto N, Sano M, Konno H, Setou M, Unno N. Loss of lymphatic vessels and regional lipid accumulation is associated with incompetent great saphenous vein incompetence. J Vasc Surg. 2012 May;55(5):1440-8.
(3) Shrivas K, Hayasaka T, Sugiura Y, Setou M.

Method for Simultaneous Imaging of Endogenous Low Molecular Weight Metabolites in mouse brain using TiO(2) nanoparticle in nanoparticle-assisted laser desorption/ionization-imaging mass spectrometry. Anal Chem. 2011 Oct 1;83(19):7283-9.
(4) Kaneko Y, Obata Y, Nishino T, Kakeya H, Miyazaki Y, Hayasaka T, Setou M, Furusu A, Kohno S. Imaging mass spectrometry analysis reveals an altered lipid distribution pattern in the tubular areas of hyper-IgA murine kidneys. Exp Mol Pathol. 2011 Oct;91(2):614-21.
(5) Kubo A, Ohmura M, Wakui M, Harada T, Kajihara S, Ogawa K, Suemizu H, Nakamura M, Setou M, Suematsu M. Semi-quantitative analyses of metabolic systems of human colon cancer metastatic xenografts in livers of superimmunodeficient NOG mice. Anal Bioanal Chem. 2011 Jun;400(7):1895-904.
(6) Zaima N, Sasaki T, Tanaka T, Cheng XW, Onoue K, Hayasaka T, Goto-Inoue N, Enomoto H, Unno N, Kuzuya M, Setou M. Imaging mass spectrometry-based histopathologic examination of atherosclerotic lesions. Atherosclerosis. 2011 Aug;217(2):427-32.

【英文総説】
(1) Goto-Inoue N, Hayasaka T, Zaima N, Setou M. Imaging mass spectrometry for lipidomics. Biochim Biophys Acta. 2011 Nov;1811(11):961-9.

【英文著書】
(1) Shrivas K, Setou M. Imaging Mass Spectrometry: Sample Preparation, Instrumentation, and Applications. Advances in IMAGING and ELECTRON PHYSICS. 2012;171:145-193.
(2) Hameed S, Sugiura Y, Kimura Y, Shrivas K, Setou M. Nanoparticle-assisted Laser Desorption/ionization [nano-PALDI]-based Imaging Mass Spectrometry [IMS] and its Application to Brain Science. Nanomedicine and the Norvous System. 2012;97-118.

【和文総説】
(1) 稲見勝朗、瀬藤光利、Imaging Mass Spectrometry（質量顕微鏡法）、Medical Science Digest、2012年1月38巻1号p5-6
(2) 瀬藤光利、生物物理の最前線　質量顕微鏡法の新展開、パリティ、2011年12月26巻12号p56-60
(3) 瀬藤光利、序論－分子イメージングの最先端の特集にあたって－、最新医学、2011年66巻10号p2289-2291

2. 学会発表
(1) 瀬藤光利、質量分析計を用いた最新のバイオマーカー、第32回日本臨床薬理学会年会、浜松、2011年12月
(2) 佐藤哲郎、白井祐輔、高橋郁太、古川省吾、脇紀彦、瀬藤光利、乳癌循環腫瘍細胞の質量顕微鏡法を用いた解析、第6回浜松医科学シンポジウム、浜松、2012年2月

H. 知的財産権の出願・登録状況
1. 特許取得
出願番号：2006-043237　登録日 2011/11/18
特許番号：4866098
タイトル：質量分析装置　発明人：竹内貞夫、小河潔、吉田佳一、瀬藤光利、新間秀一

2. 実用新案登録
該当なし

3.その他
該当なし

研究成果の刊行に関する一覧表

雑誌 【原著論文】

発表者氏名	論文タイトル名	発表誌名	巻号	ページ	出版年
Yamada M, Yao I, Hayasaka T, Ushijima M, Matsuura M, Takada H, Shikata N, Setou M, Kwon KH, Ito S.	Identification of oligosaccharides from histopathological sections by MALDI imaging mass spectrometry.	Anal Bioanal Chem.	402(5)	1921-30	2012 Feb
Tanaka H, Zaima N, Sasaki T, Yamamoto N, Sano M, Konno H, Setou M, Unno N.	Loss of lymphatic vessels and regional lipid accumulation is associated with incompetent great saphenous vein incompetence.	J Vasc Surg.	55(5)	1440-8	2012 May
Shrivas K, Hayasaka T, Sugiura Y, Setou M.	Method for Simultaneous Imaging of Endogenous Low Molecular Weight Metabolites in mouse brain using TiO(2) nanoparticle in nanoparticle-assisted laser desorption/ionization-imaging mass spectrometry.	Anal Chem.	83(19)	7283-9	2011 Oct
Kaneko Y, Obata Y, Nishino T, Kakeya H, Miyazaki Y, Hayasaka T, Setou M, Furusu A, Kohno S.	Imaging mass spectrometry analysis reveals an altered lipid distribution pattern in the tubular areas of hyper-IgA murine kidneys.	Exp Mol Pathol.	91(2)	614-21	2011 Oct
Kubo A, Ohmura M, Wakui M, Harada T, Kajihara S, Ogawa K, Suemizu H, Nakamura M, Setou M, Suematsu M.	Semi-quantitative analyses of metabolic systems of human colon cancer metastatic xenografts in livers of superimmunodeficient NOG mice.	Anal Bioanal Chem.	400(7)	1895-904	2011 Jun
Zaima N, Sasaki T, Tanaka T, Cheng XW, Onoue K, Hayasaka T, Goto-Inoue N, Enomoto H, Unno N, Kuzuya M, Setou M.	Imaging mass spectrometry-based histopathologic examination of atherosclerotic lesions.	Atherosclerosis.	217(2)	427-32	2011 Aug

雑誌【英文総説】

発表者氏名	論文タイトル名	発表誌名	巻号	ページ	出版年
Goto-Inoue N, Hayasaka T, Zaima N, Setou M.	Imaging mass spectrometry for lipidomics.	Biochim Biophys Acta.	1811(11)	961-9.	2011 Nov

書籍【英文著書】

著者氏名	論文タイトル名	書籍全体の編集者名	書　籍　名	出版社名	出版地	出版年	ページ
Shrivas K, Setou M.	Imaging Mass Spectrometry: Sample Preparation,Instrumentation, and Applications.	Peter W. Hawkes	Advances in IMAGING and ELECTRON PHYSICS.	Elsevier	Amsterdam	2012	145-193.
Hameed S,Sugiura Y, Kimura Y, Shrivas K, Setou M.	Nanoparticle-assisted Laser Desorption/ionization [nano-PALDI]-based Imaging Mass Spectrometry [IMS] and its Application to Brain Science.	Colin R.Martin, Victor R.Preedy, Ross J.Hunter	Nanomedicine and the Nervous System.	CRC Press	London	2012	97-118

雑誌【和文総説】

発表者氏名	論文タイトル名	発表誌名	巻号	ページ	出版年
稲見勝朗、瀬藤光利	Imaging Mass Spectrometry(質量顕微鏡法)	Medical Science Digest	38巻1号	5-6	2012
瀬藤光利	生物物理の最前線　質量顕微鏡法の新展開	パリティ	26巻12号	56-60	2011
瀬藤光利	序論－分子イメージングの最先端の特集にあたって－	最新医学	66巻10号	2289-2291	2011

Identification of oligosaccharides from histopathological sections by MALDI imaging mass spectrometry

Masanori Yamada, Ikuko Yao, Takahiro Hayasaka, Masaru Ushijima, Masaaki Matsuura, Hideho Takada, Nobuaki Shikata, Mitsutoshi Setou, et al.

Analytical and Bioanalytical Chemistry

ISSN 1618-2642

Anal Bioanal Chem
DOI 10.1007/s00216-011-5622-y

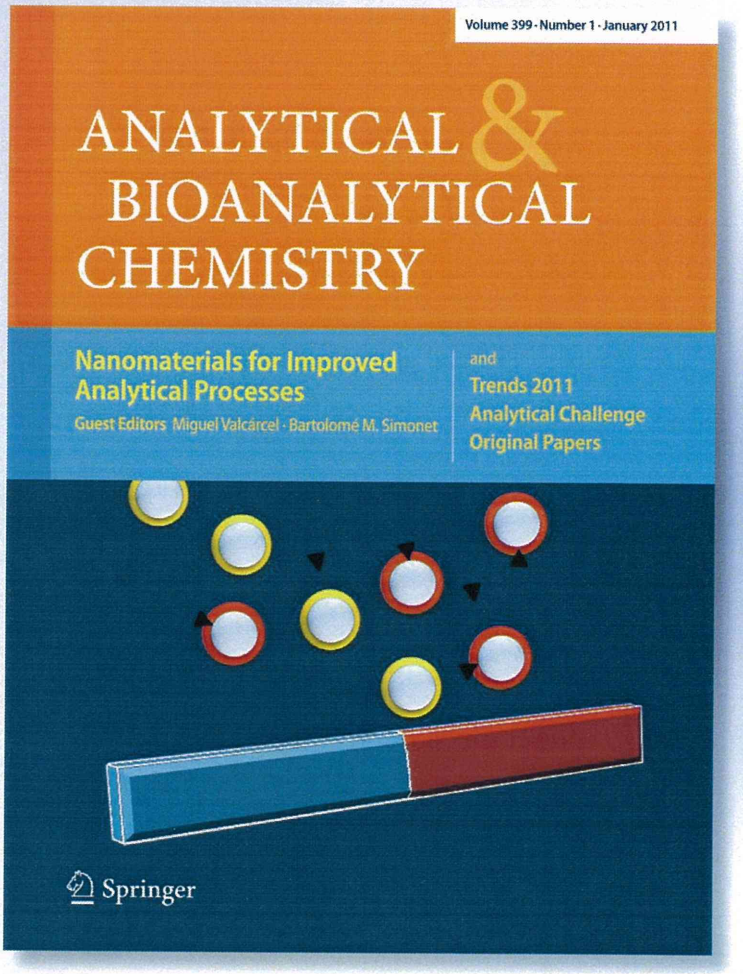

Springer

Anal Bioanal Chem
DOI 10.1007/s00216-011-5622-y

ORIGINAL PAPER

Identification of oligosaccharides from histopathological sections by MALDI imaging mass spectrometry

Masanori Yamada · Ikuko Yao · Takahiro Hayasaka · Masaru Ushijima · Masaaki Matsuura · Hideho Takada · Nobuaki Shikata · Mitsutoshi Setou · A-Hon Kwon · Seiji Ito

Received: 28 September 2011 / Revised: 28 November 2011 / Accepted: 28 November 2011

Abstract Direct tissue analysis using matrix-assisted laser desorption/ionization (MALDI) mass spectrometry (MS) provides the means for in situ molecular analysis of a wide variety of biomolecules. This technology—known as imaging mass spectrometry (IMS)—allows the measurement of biomolecules in their native biological environments without the need for target-specific reagents such as antibodies. In this study, we applied the IMS technique to formalin-fixed paraffin-embedded samples to identify a substance(s) responsible for the intestinal obstruction caused by an unidentified foreign body. In advance of IMS analysis, some pretreatments were applied. After the deparaffinization of sections, samples were subjected to enzyme digestion. The sections co-crystallized with matrix were desorbed and ionized by a laser pulse with scanning. A combination of α-amylase digestion and the 2,5-dihydroxybenzoic acid matrix gave the best mass spectrum. With the IMS Convolution software which we developed, we could automatically extract meaningful signals from the IMS datasets. The representative peak values were *m/z* 1,013, 1,175, 1,337, 1,499, 1,661, 1,823, and 1,985. Thus, it was revealed that the material was polymer with a 162-Da unit size, calculated from the even intervals. In comparison with the mass spectra of the histopathological specimen and authentic materials, the main component coincided with amylopectin rather than amylose. Tandem MS analysis proved that the main components were oligosaccharides. Finally, we confirmed the identification of amylopectin by staining with periodic acid-Schiff and iodine. These results for the first time show the advantages of MALDI-IMS in combination with enzyme digestion for the direct analysis of oligosaccharides as a major component of histopathological samples.

M. Yamada · H. Takada · A.-H. Kwon
Department of Surgery, Kansai Medical University,
2-3-1 Shin-machi,
Hirakata, Osaka 573-1191, Japan

I. Yao · S. Ito
Department of Medical Chemistry, Kansai Medical University,
10-15 Fumizono-cho,
Moriguchi, Osaka 570-8506, Japan

I. Yao (✉)
Precursory Research for Embryonic Science and Technology (PRESTO), Japan Science and Technology Agency (JST),
7 Goban-cho,
Chiyoda-ku, Tokyo 102-0076, Japan
e-mail: yaoik@takii.kmu.ac.jp

T. Hayasaka · M. Setou
Department of Molecular Anatomy,
Hamamatsu University School of Medicine,
1-20-1 Handayama, Higashi-ku,
Hamamatsu, Shizuoka 431-3192, Japan

M. Ushijima · M. Matsuura
Bioinformatics Group, Genome Center,
Japanese Foundation for Cancer Research,
3-8-31 Ariake,
Koto-ku, Tokyo 135-8550, Japan

M. Matsuura
Division of Cancer Genomics, Cancer Institute,
Japanese Foundation for Cancer Research,
3-8-31 Ariake,
Koto-ku, Tokyo 135-8550, Japan

N. Shikata
Department of Clinical Sciences and Laboratory Medicine,
Kansai Medical University,
10-15 Fumizono-cho,
Moriguchi, Osaka 570-8506, Japan

Published online: 13 December 2011

Keywords Imaging mass spectrometry · MALDI-TOF MS · Bioanalytical methods · Amylase · Amylopectin · Oligosaccharide

Abbreviations

DHB	2,5-Dihydroxybenzoic acid
FFPE	Formalin-fixed paraffin-embedded
HE	Hematoxylin and eosin
IMS	Imaging mass spectrometry
ITO	Indium tin oxide
MALDI	Matrix-assisted laser desorption/ionization
PAS	Periodic acid-Schiff stain
ROI	Region of interest
CT	Computed tomography

Introduction

Recently, imaging mass spectrometry (IMS) has emerged and was dramatically developed for proteomic and metabolomic analyses [1, 2] in many fields including biology [3, 4] and pathology [5, 6]. Direct tissue analysis using matrix-assisted laser desorption/ionization (MALDI)-MS provides the means for the in situ molecular analysis of a wide variety of biological molecules. In IMS, the mass spectra associated with spatial information can be continuously recorded to obtain the expression patterns of various molecules in the specimens to be analyzed [7–11]. With this technique, we can perform MS directly from tissue sections and analyze biological compounds [12–14]. This technology allows the measurement of these species without the need for target-specific reagents such as antibodies [15, 16]. MALDI-IMS enables us to obtain the molecular constituents of the object substance along with local information of various unknown components in a single measurement. In recent years, a great many advances in the practice of IMS have occurred, making the technique more sensitive and useful [17]. A major advantage of direct MALDI analysis is that it avoids time-consuming extraction, purification, or separation steps, which have the potential of producing artifacts. One of the recent applications of MALDI MS is its use to profile and image components directly from tissue sections [7, 18].

We and other groups have proposed methods for performing in situ proteomic analyses by IMS as an additional efficient technique for proteomic analysis to two-dimensional electrophoresis [1, 15, 16]. Moreover, IMS procedure has begun to be used for formalin-fixed paraffin-embedded (FFPE) samples that are commonly used in hospitals and stored for a long time [19]. Here, we applied the IMS technique for FFPE histological analyses of the substance of intestinal obstruction material.

Bowel obstruction or intestinal obstruction is a mechanical or functional obstruction of the intestine that prevents the normal transit of digested materials. It can occur at any levels distal to the duodenum of the small intestine and is typically considered to represent a medical emergency. For the case in this study, surgery was needed to remove the necrotic tissue and causative materials. Even after the materials were removed, the cause and the identity of the materials were not clarified. To obtain information of the extirpated materials, the IMS technique was employed.

Methods

Materials

Human sample analysis in this study was started after approval of the ethical committee of Kansai Medical University and followed the committee's requests regarding informed consent.

α-Amylase (A0521, 1,000–1,500 U/mg, lyophilized powder, derived from human saliva) was purchased from Sigma-Aldrich (St. Louis, MO, USA). Calibration standard peptides and 2,5-dihydroxybenzoic acid (DHB) were purchased from Bruker Daltonics (Leipzig, Germany). Iodine and potassium iodide were obtained from Yoshida Pharmaceutical Co. Ltd. (Tokyo, Japan) and Merck (Darmstadt, Germany), respectively. The traditional rice cake known as *mochi* in Japan, which is made from glutinous rice, was purchased from a local market. Starches made from rice, potato, wheat, and corn were also obtained in the local market. High-amylose starch was obtained from Nihon Shokuhin Kako Co. Ltd. (Tokyo, Japan).

Diagnosis, examinations, and operations of intestinal obstruction

In the physical examination, localized tenderness was identified in the umbilical region. After computed tomography (CT) scanning, the pain had progressed severely and there was rebound tenderness and muscle guarding in the same area. Contrast-enhanced CT showed the high-density mass in the dilated small intestine and air fluid level formation in the right iliac fossa. Laparoscopic operation was performed to excise the inflamed small intestine and the obstructive material. The laparoscopy-assisted operation was performed with a three-port system. Serous and yellow ascites were present in the right iliac fossa and not inflamed in the appendix, gallbladder, ovaries, and other organs in the abdominal cavity. A foreign body was detected in the dilated and inflamed ileum at 100 cm from the ileum end. That small intestine was resected with assisted laparoscopy. The surgically isolated intestinal portion and the foreign body

were fixed and paraffin-embedded as performed routinely at Kansai Medical University Hospital and then subjected to IMS analysis.

Sample preparation with on-tissue digestion

The samples in paraffin blocks were cut into 4-μm sections and mounted onto an indium tin oxide (ITO)-coated glass slide (Bruker Daltonics). Paraffin was removed with xylene from the sample to give the enzyme complete access to the sample followed by crystallization with matrix. In detail, before clearing, the samples were heated to melt the paraffin and then washed multiple times with xylene to remove the paraffin. Xylene was removed and the sample was rehydrated by graded washes with xylene and ethanol, and then through graded washes of ethanol in water, ending in a final rinse in pure water. Deparaffinized sections on an ITO-coated glass slide were subjected to a small amount of enzyme digestion using 10 U/mL of α-amylase in 0.1 M phosphate buffer (pH 6.4) at 37 °C for 2 h in a humidified chamber so as not to disrupt the configuration of the components in the sample. Glass slides were dried using a SpeedVac vacuum at room temperature. The matrix solution containing 50 mg/mL of DHB in 70% methanol and 0.1% trifluoroacetic acid was uniformly sprayed over the samples using a 0.2-mm nozzle caliber airbrush (Procon Boy FWA Platinum, Mr. Hobby, Tokyo, Japan), and the same solution was dropped onto a portion of the section. The samples were subjected to laser scanning for MALDI-IMS or tandem mass spectrometry (MS/MS).

As a reference, a small portion of *mochi* (about 5×5×10 mm) or boiled dumplings containing high-amylose starch was fixed with 4% paraformaldehyde and treated according to the same procedure used to prepare the histopathological sample. The *mochi* and dumpling samples were then subjected to direct MALDI-MS analyses.

Imaging mass spectrometry

We adopted the procedures for MALDI-IMS described previously [6, 12], with some modifications. After applying the coating matrix, the histopathological sections were analyzed using a MALDI-TOF/TOF-type instrument, Ultraflex II (Bruker Daltonics), which was equipped with a 355-nm Nd:YAG laser. A 200-Hz repetition rate was used. Data were acquired in the positive ion mode using an external calibration method. Calibration proteins were deposited on the surfaces of sample support materials to minimize mass shift. The interval between data points was 50 μm, and 100 shots of laser beam were irradiated on each data point. The IMS dataset acquired by a Mass Microscope (Shimadzu, Kyoto, Japan) was converted to analyze the format file to enable analysis with the BioMap free software and the IMS Convolution software, which we have developed, as well as Bruker's software.

Data analysis

To extract the *m/z* values of the major peaks, we used our custom-designed IMS Convolution software with the common peak method [20]. For peak detection, we set a *k*-nearest neighborhood as a width of window on the *x*-axis (or *m/z*-axis); an *m/z* value achieving the maximum intensity in each window is regarded as a peak. The window is moved along the *x*-axis and the peaks are searched in the mass spectrum of each measurement point. Moreover, we set two regions of interest (ROIs) on the histopathological sample and outside using an optical image corresponding to the entire measurement area. The optical image was automatically extracted using a Mass Microscope. The IMS Information software, which is also custom-designed, is produced by Shimadzu Co. The settings of window size and the divided number are optimized to automatically set ROIs on an optical image. The area information output is provided as a text format and loaded into IMS Convolution. The common peaks are searched within each area. Common peaks are defined by the point x in which an average of peaks, $A(x)$, is greater than a certain threshold, h. Here, the $A(x)$ of ROI r, say $A_r(x)$, was calculated by averaging Gaussian kernels with center at the individual peak, as expressed follows:

$$A_r(x) = \frac{1}{N_r} \sum_{i=1}^{N_r} \sum \exp\left[-\frac{(x - p_{ij})^2}{(\sigma p_{ij})^2} \right].$$

where N_r is the number of data points in ROI r, p_{ij} is the *m/z* value of the ith subject's jth peak, and σ is a parameter accounting for the width of the peak. The common peaks are listed on each area in the csv format file and used to reconstruct the ion images using BioMap. The maximum values to reconstruct ion images were optimized to be clear.

Image reconstruction

Image reconstruction from signals in the spectra was performed using FlexImaging (Bruker Daltonics) as previously described [12]. Because the ionization efficiency could vary depending on the matrix–analyte co-crystallization conditions and their sublimation during measurement [12, 15], the absolute intensities of the mass spectra were normalized to the same value of total ion current to eliminate the variations of ionization efficiency. After the normalization process, ion images were reconstructed from signals in the spectra using FlexImaging.

MS/MS analyses

Tandem mass spectrometry analysis was performed using a Mass Microscope (Shimadzu). The Nd:YAG laser was run at 1,000 Hz and the mass spectra were mainly obtained from 200 laser shots per measurement point. In the MS/MS operation, the data acquisition conditions (i.e., the laser power, collision energy, and number of laser irradiations) were optimized in order to obtain product ion mass spectra with high signal-to-noise ratios (S/N) of the fragment peaks.

Special staining of paraffin section

The paraffin section samples were prepared and then deparaffinized sections were subjected to general or special histopathological staining. Hematoxylin–eosin (HE) staining, periodical acid-Schiff (PAS), PAS diastase (D-PAS) [21], Alcian blue, Kossa, Dylon, and Congo red staining were performed. S-100 protein detection, immunostaining with anti-S100 antibody, was performed. To detect human macrophages, CD68 immunostaining [22] was carried out. Silver impregnation was also conducted. These staining procedures were conducted according to established methods for histopathological examination at the Department of Clinical Sciences and Laboratory Medicine in Kansai Medical University. For the iodide reaction, 2% iodine and 4% potassium iodide solution was used at room temperature.

Results and discussion

Workflow of the sample preparation with enzyme digestion for IMS

For IMS analysis, the outline of the procedure for direct mass imaging in this study is shown in Fig. 1. The affected region of the small intestine and the foreign substances were removed with laparoscopic assistance (Fig. 1a). Surgically isolated intestine and the foreign body were fixed and paraffin-embedded as routinely performed at the Kansai Medical University Hospital. The histopathological sections were prepared from FFPE blocks of the removed intestine and the foreign body. Then, the 4-μm sections were extended on ITO-coated glass slides. Deparaffinized sections on ITO-coated glass slides were subjected to IMS analysis (Fig. 1b). First, we tried to obtain the mass spectra without any pretreatment; no signals were found. Since we did not have information about the constituents of the foreign body, we then tried to make

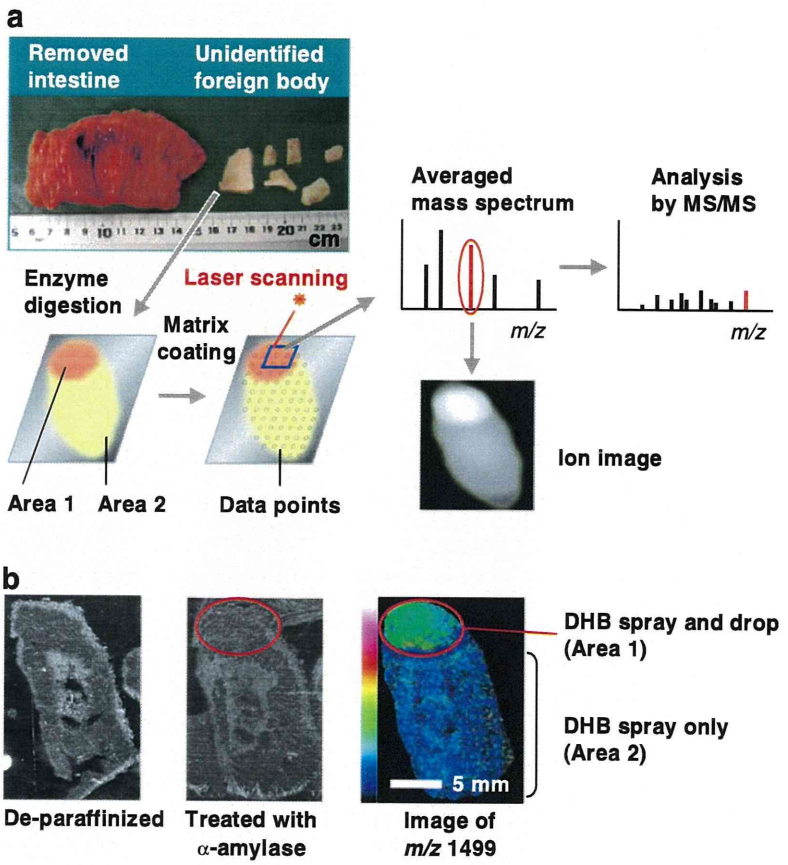

Fig. 1 Overview of the imaging mass spectrometry (IMS) procedure. **a** Appearance of the isolated portion of the surgically removed small intestine and the unidentified foreign body (*upper panel*) and the workflow of sample preparation for IMS. Samples in the paraffin blocks were sliced into 4-μm-thin sections, mounted on ITO-coated slide glasses, and then deparaffinized. After digestion with α-amylase, the samples were coated with DHB matrix by uniform spraying and addition of droplets. The well-dried samples on the slide were subjected to laser scanning for MALDI-IMS followed by ion image reconstruction. The spectra of particular interest (*red line*) were examined by tandem mass spectrometry. **b** Samples at three stages of the IMS procedure. The *red circle* designated as "*Area 1*" shows the region added with the DHB droplet. The other region is termed "*Area 2*"

fragmentation of the material with enzyme digestion (Fig. 1b). We applied amylase for carbohydrate- or oligosaccharide-like materials and trypsin for protein-like materials. Then, the matrix solution was sprayed on the section samples. For the samples that were not treated with α-amylase or without matrix addition, we hardly detected or did not obtain any signals upon laser exposure (data not shown). Because the spray droplet method [12] enhances the ionization efficiency for MALDI-IMS, a small amount of matrix solution was dropped onto the slide after the DHB spray (area 1, red circle in Fig. 1b). The slide was then dried and subjected to IMS analysis. In total, stronger signals were detected in area 1 than in area 2. For example, the signal intensity of the molecule represented by *m/z* 1499 was higher in area 1 (Fig. 1b); other molecules had high signal intensities in the area (Figs. 2 and 3). Thus, we mainly focused on area 1 for subsequent analyses.

Direct mass imaging analysis of the histopathological section

After data acquisition, the IMS dataset was converted to the ANALYZE 7.5 format file for loading to BioMap, as described previously [13], and to our custom-designed IMS Convolution software [23]. The peaks were extracted from the large IMS dataset manually with BioMap and automatic procedures with the IMS Convolution software, with information on ROIs such as areas 1 and 2. When the peaks were extracted manually from the averaged mass spectrum of all spots in area 1 from the BioMap peak pattern, the averaged mass spectra were provided as output in text format files and labeled one by one (Fig. 2a). To automatically extract the meaningful *m/z* values of the major peaks with ROI information from the IMS datasets, we applied the IMS Convolution software. The processing is based on the detection of "common peaks" [20] within the ROIs. With the IMS Convolution software, the peak values in areas 1 and 2 were automatically extracted and exported as a text file. The calculated values designated as common peaks were plotted in the graph, which reflected the frequency of appearance and the signal intensities (Fig. 2b).

The molecule represented by *m/z* 1,175 was detected with the highest intensity (Fig. 2a), and the molecule represented by *m/z* 1,337 was detected at the highest frequency (Fig. 2b). A few peaks were detected from area 2 (Fig. 2c). The spectral patterns shown in Fig. 2 suggest that the foreign body was composed of polymers. Moreover, the pitch width of each major peak was *m/z* 162 (Table 1). Other peaks were also observed, such as isotopic signals ([M+1] and [M+2], details not shown), sodium adduct ($[M + Na]^+$), and potassium adduct ($[M + K]^+$), judged from the differences of the *m/z* values from major peaks. The signal intensities of $[M + Na]^+$ were higher than $[M + K]^+$, mainly

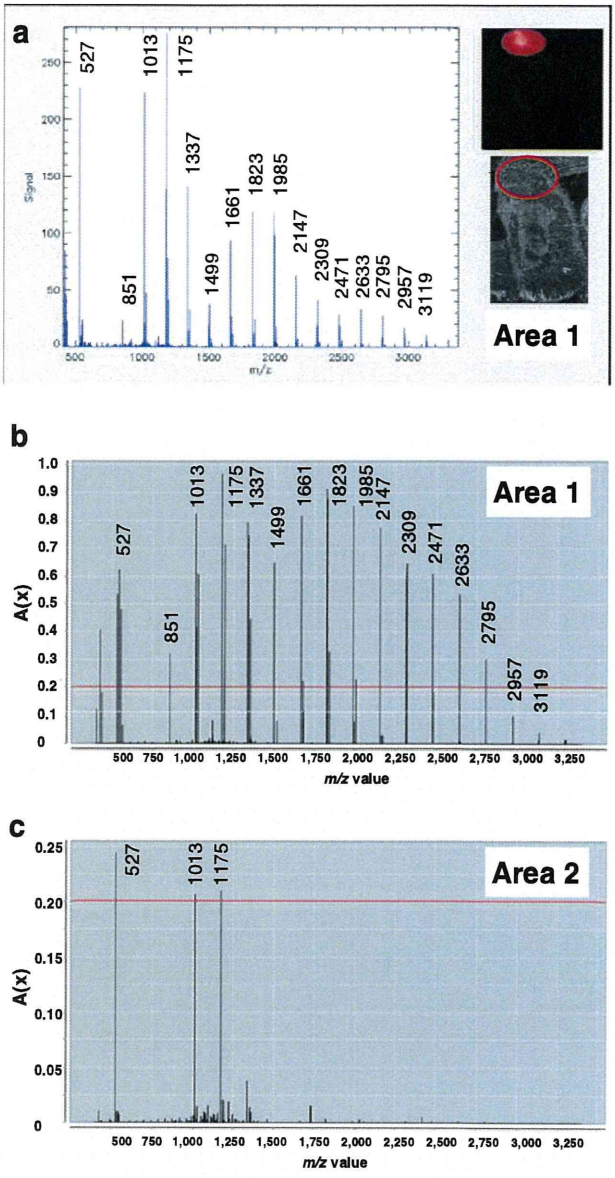

Fig. 2 Peaks obtained from the histopathological paraffin section by IMS. **a** Average of spectra of area 1 drawn using BioMap software. Major peaks were selected and the indicated *m/z* values were labeled manually. **b**, **c** Peaks of areas 1 and 2 extracted using the IMS Convolution software. The major peaks are extracted as common peaks and displayed as the spectra of $A(x)$. The threshold value is indicated by the *red lines* at 0.2

because sodium phosphate buffer was used for enzyme digestion.

Image reconstruction of the histopathological section

The distribution patterns of some ions which had *m/z* 162 intervals were reconstructed from the IMS data (Fig. 3). Those were picked up by the $A(x)$ value 0.2 as thresholds, except for large molecules at *m/z* 2,957 and at *m/z* 3,119.

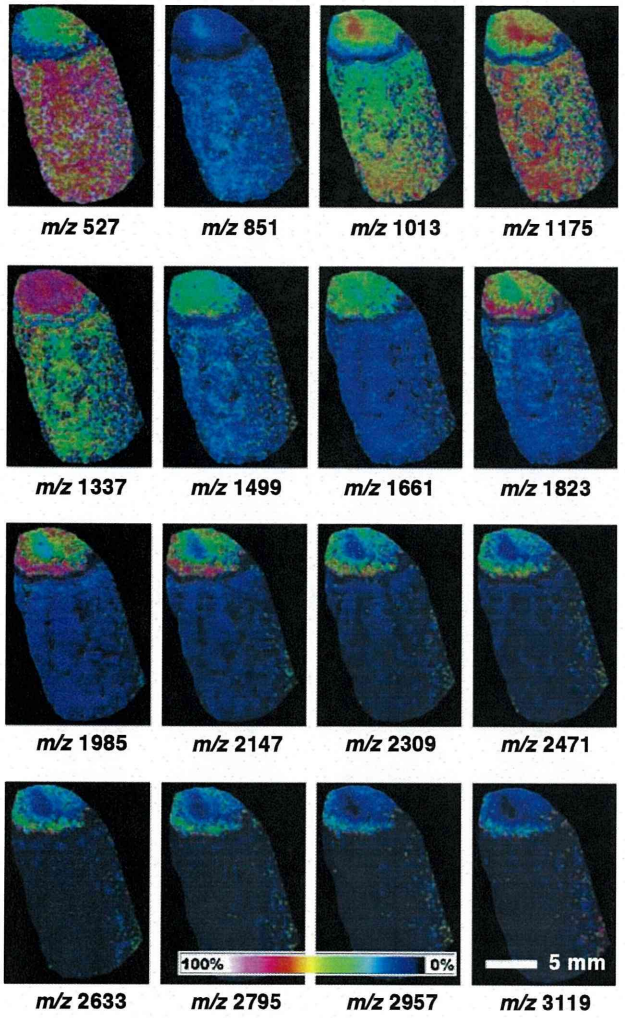

Fig. 3 Imaging mass spectrometry analyses of the histopathological paraffin section. Reconstructed images of the major peaks of area 1 extracted by the IMS Convolution software shown in Fig. 2b and Table 1. The signal intensity is shown in *pseudo-rainbow-colored images*

Reconstructed ion images in Fig. 3 show that the spray droplet method [12] was effective for ionization of a wide variety of *m/z* molecules, from *m/z* 527 to *m/z* 3,119, especially for the high *m/z* value region. The abundance of each molecule detected in areas 1 and 2 was not parallel. For example, ion at *m/z* 1,337 was most abundant in area 1, whereas ion at *m/z* 527 was the main signal in area 2. The results show that the efficiency of ionization could be changed by the *m/z* value, abundances of the analytes, and the ionization procedure of how to make an analyte–matrix complex.

Comparison with amylopectin and high-amylose starch

Because enzyme treatment gave good quality mass spectra, it was suggested that the component of the foreign body was oligosaccharide, the substrate of α-amylase. α-Amylase (EC# 3.2.1.1) is an endo-type 1,4-α-D-glucan glucanohydrolase; maltose and polysaccharides with more than three residues of glucose are produced. A representative substrate of α-amylase, starch is classified into amylose and amylopectin. Natural starches are a mixture of amylose (10–20%) and amylopectin (80–90%). The traditional rice cake known as *mochi* in Japan, which is made from glutinous rice, is entirely composed of amylopectin.

We compared the spectral pattern of the histopathological section with those of an authentic *mochi* sample (no amylose and 100% amylopectin) and some kinds of starch containing various rates of amylose. Common rice starch contains 15–20%, potato starch and wheat starch have 20–25%, corn starch contains 25%, and high-amylose starch contains about 50% amylose. The reference materials were treated with the same procedures as the histopathological sample and analyzed with direct MALDI-MS analyses. The spectral patterns of starch containing amylose and *mochi* were different, and that of the histopathological sample coincided with the latter (Fig. 4). Both the histopathological

Table 1 Extracted common peaks of areas 1 and 2

A(*x*)	Major peaks (*m/z*)	Peaks (*m/z*)	Interval of major peaks (*m/z*)	Differences between the head peaks (*m/z*)
0.53	527	527	104	
0.62		*543*		16
0.32	851	851	324	
0.82	1,013	1,013	162	
0.61		*1029*		16
0.97	1,175	1,175	162	
0.68		*1,191*		16
0.71	1,337	1,337	162	
0.44		*1,353*		16
0.65	1,499	1,499	162	
0.82	1,661	1,661	162	
0.24		*1,677*		16
0.82	1,823	1,823	162	
0.22		*1,840*		16
0.91	1,985	1,985	162	
0.79	2,147	2,147	162	
0.65	2,309	2,309	162	
0.54	2,471	2,472	162	
0.43	2,633	2,633	162	
0.30	2,795	2,795	162	
	2,957	2,957	162	
	3,119	3,119	162	
0.24	(Area 2)	527		
0.21	(Area 2)	1,013	486	
0.21	(Area 2)	1,175	162	

Values in italics are derived from $[M + K]^+$

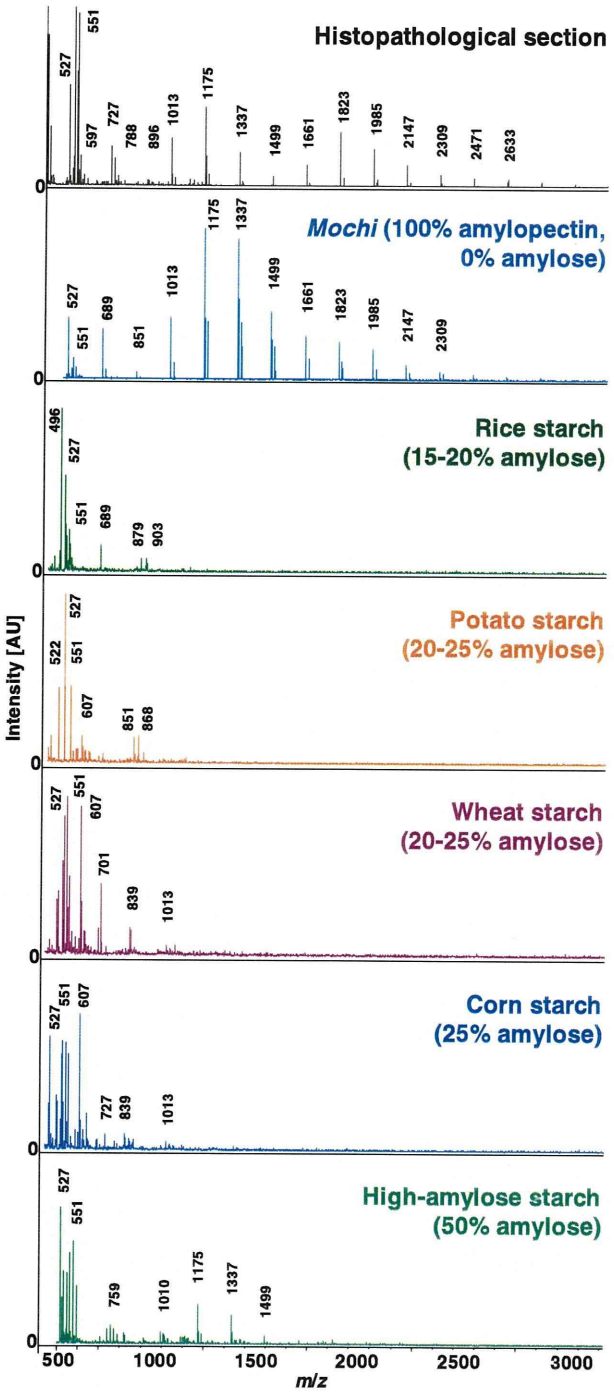

Fig. 4 Comparison of mass spectra with amylopectin and amylose. The mass spectra were obtained from the pathological section of the foreign body and authentic materials prepared from *mochi* and various kinds of starch. *Mochi* has no amylose, whereas other starches have different contents of amylose. All samples were subjected to α-amylase digestion and attached to the DHB matrix. Signals were obtained using UltraFlex II. Signal intensities in the graph were determined by relative intensity with arbitrary unit (*AU*)

sample and authentic *mochi* had polymer-like signals to the relatively large mass range, whereas other starches did not have such even interval signals (Fig. 4). This may be explained by the notion that amylopectin is difficult to be digested by α-amylase due to the α-(1-6)-D-glycopyranosyl branches. Other starches had signals with lower *m/z* regions, suggesting that the pretreatment with α-amylase digested extensively glucose linkages. These results provide strong evidence that the material causing the obstruction was *mochi*. Treatment with α-amylase produced many peaks at essentially equidistant intervals with an *m/z* value of 162. The maximum *m/z* value detected was 3,119, which

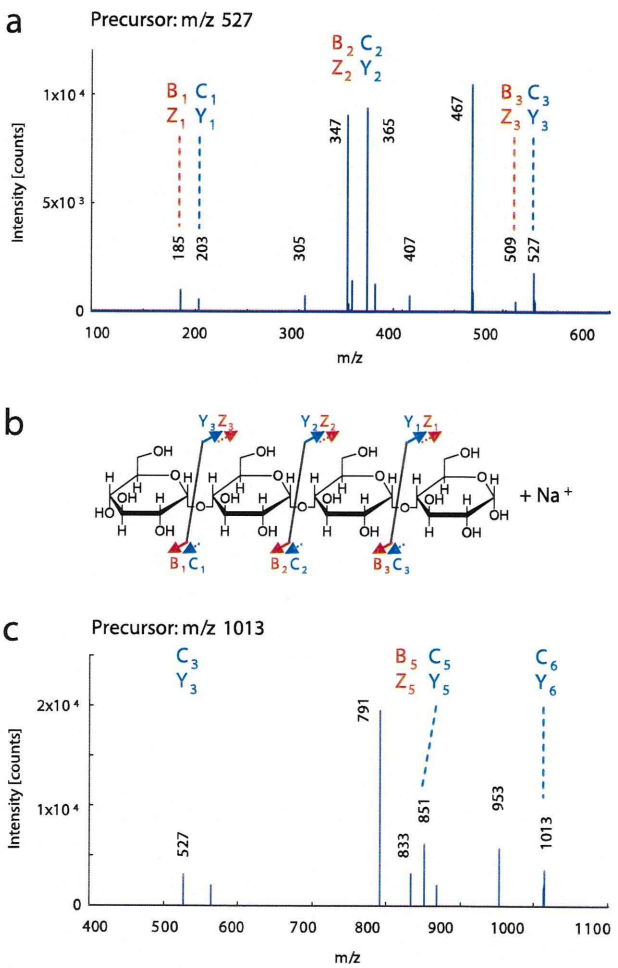

Fig. 5 Tandem mass spectrometry of polyglucose from the paraffin sections of the foreign body. **a** The ions of the diagnostic fragments suggest that the ions at *m/z* 527 are from polyglucose. Direct MS/MS spectrum of the precursor ion at *m/z* 527—fragmentations of the ions of 4-mer oligosaccharides. **b** Nomenclature of fragment ions and scheme of the observed glycosidic cleavages. **c** Direct MS/MS spectrum of the precursor ion at *m/z* 1,013—fragmentations of the ions of 6-mer oligosaccharides. Tandem mass spectrometry experiments were performed with a Mass Microscope. Signal intensities in the graph were determined by the MS count (**a**, **c**)

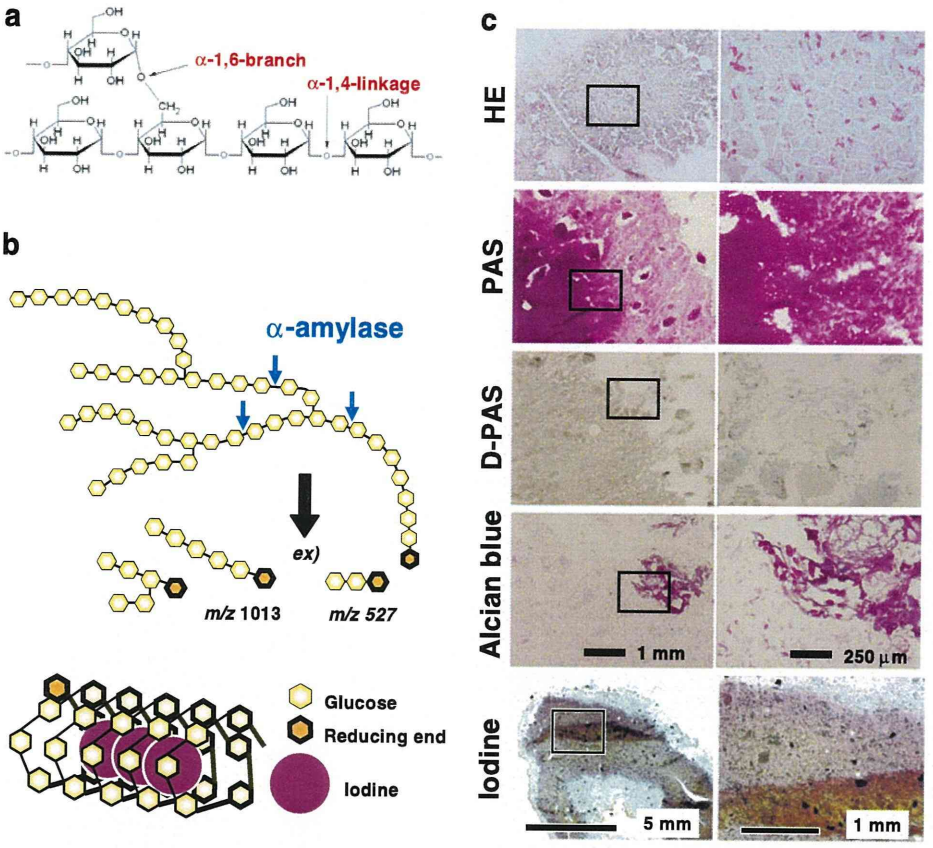

Fig. 6 Reaction of the paraffin sections of the foreign body with iodine. **a** Structure of the α-1,4-linkages and the α-1,6-branch of glucose oligosaccharides. **b** Schematic representation of the enzyme digestion of glucose polysaccharide by α-amylase and the iodide reaction in spires of polysaccharide with α-1,4-linkages. The drawing sizes of the molecules do not reflect the actual ones. **c** Histopathological staining of the paraffin sections of the foreign body. Results of hematoxylin and eosin (*HE*), periodical acid-Schiff (*PAS*), PAS diastase treatment (*D-PAS*), Alcian blue, and iodine stainings are shown. The *right panels* show fourfold magnified images of the respective left panel. In the iodine reaction, *light brown to red purple colors* indicate the presence of oligosaccharide or starch. The strong brown color may be due to the overlap of the sections. The *right panel* shows fourfold magnified image of the boxed region of the left panel

corresponded to the sodium adduct of a polysaccharide having 16 glucose residues (Figs. 2 and 4 and Table 1).

Tandem mass spectrometry of polyglucose in the histopathological paraffin sections

We further investigated the obstruction material using tandem MS (MS*n*) to confirm that the fragment ions were derived from oligosaccharides. First, the direct MS/MS spectrum of the precursor ion at *m/z* 527 was analyzed. The value of *m/z* was identical to that of the sodiated oligosaccharide. In the MALDI-MS/MS experiments using the Mass Microscope, the degradation of carbohydrates formed ion series that included B- and Y-type ion cleavages (nomenclature system of [24]). These ion series are formed by the subsequent loss of the incremental mass of monosaccharides; thus, the ion series for amylose showed a mass difference of 162. We identified the one (C or Y) series oligosaccharides represented by 2-mer ions at *m/z* 203 ($C_6H_{12}O_6$, $[M + Na]^+$) and 3-mer at *m/z* 365 ($C_{12}H_{22}O_{11}$, $[M + Na]^+$; Fig. 5a, b). These results suggest that maltotriose signal with sodium ion ($C_{36}H_{66}O_{33}$, $[M + Na]^+$) was detected as ion at *m/z* 527. Peaks derived from a second (B or Z) series ions were also detected as ions at *m/z* 185, *m/z* 347, and at *m/z* 509 (Fig. 5a, b).

In a similar manner, we detected the direct MS/MS spectrum of the precursor ion at *m/z* 1,013, which was also expected to be a sodiated oligosaccharide. The glucose polymer comprises 5-mer oligosaccharides with sodium ion as a C- or Y-type fragment ion ($C_{30}H_{50}O_{25}$, $[M + Na]^+$, *m/z* 851); the B- or Z-type fragment ions ($C_{30}H_{48}O_{24}$, $[M + Na]^+$, *m/z* 833) were detected along with maltotriose as their ion $[M + Na]^+$ located at *m/z* 527. Thus, the ions of the diagnostic fragments suggest that the ion at *m/z* 1,013 and 527 originate from a polysaccharide or an oligosaccharide (Fig. 5).

Identification of oligosaccharides as a glucose polymer

The *m/z* value of 162 is equivalent to that of dehydrated hexose. If the polymers consisted of α-(1-4)-D-glycopyranosyl units, the main component could be starch and/or glycogen. Such polyglucose sometimes contains α-(1-6)-D-glycopyranosyl branching, as illustrated in Fig. 6a.

We could not assume from the HE staining what would be the component. To confirm the existence of oligosaccharides, we performed conventional histopathological staining of the foreign body (Fig. 6b). PAS staining, used for the detection of sugar or glycogen in the tissue [21], gave strong signals. The PAS-positive signals disappeared after D-PAS treatment (Fig. 6b). These results of PAS staining confirmed the presence of glycogen or other carbohydrate substances. Alcian blue staining, which is usually used for mucin polysaccharide detection, showed weak and irregular signals partly throughout the whole region (Fig. 6c). Following multiple special stainings, Kossa staining for bone, Dylon and Congo red staining for amyloid, S100 for protein, CD68 for human macrophages [22], and silver impregnation for fabric were performed; all of the results were negative (data not shown). Finally, we performed iodine staining. The section was colored brown to red purple and the outside was translucent (Fig. 6c), which indicate the presence of oligosaccharide or starch. In the reaction, iodine colors inside the polysaccharide chain with α-1,4-linkages to the number of the spires. Amylose (only α-1,4-linkages) colors deep blue to purple. Amylopectin has approximately 4% α-(1-6)-D-glycopyranosyl branching. Glycogen has a higher frequency of branches and shorter length than amylopectin. The outer portions of this material appeared translucent, probably because the amylose chain was less than 12 residues in length due to the digestive action in the intestine. The iodide reaction also supported that the foreign material was *mochi*.

Conclusions

With direct MALDI-TOF MS imaging, we identified *mochi* as the obstructing material in small intestinal obstruction. The results in this study indicate that IMS is a very rapid and accurate technique with high sensitivity for the direct analysis of histopathological samples. This is the first case of the identification of oligosaccharides as the main components of histopathological samples using direct MS analyses. MALDI-TOF MS in combination with enzyme digestion will provide support for histopathological study.

Acknowledgments We thank Hosaka K, Saitou A, and Tarumi T for their assistance. We also thank Prof. Sugimura and lab members. This study is supported by Research Grants for PRESTO and SENTAN from Japan Science and Technology Agency to I. Yao.

References

1. Yao I, Sugiura Y, Matsumoto M, Setou M (2008) In situ proteomics with imaging mass spectrometry and principal component analysis in the Scrapper-knockout mouse brain. Proteomics 8 (18):3692–3701
2. Sugiura Y, Setou M (2010) Imaging mass spectrometry for visualization of drug and endogenous metabolite distribution: toward in situ pharmacometabolomes. J Neuroimmune Pharmacol 5 (1):31–43. doi:10.1007/s11481-009-9162-6
3. Bernier UR, Kline DL, Barnard DR, Schreck CE, Yost RA (2000) Analysis of human skin emanations by gas chromatography/mass spectrometry. 2. Identification of volatile compounds that are candidate attractants for the yellow fever mosquito (*Aedes aegypti*). Anal Chem 72(4):747–756
4. Garrett TJ, Yost RA (2006) Analysis of intact tissue by intermediate-pressure MALDI on a linear ion trap mass spectrometer. Anal Chem 78(7):2465–2469
5. Drexler DM, Garrett TJ, Cantone JL, Diters RW, Mitroka JG, Prieto Conaway MC, Adams SP, Yost RA, Sanders M (2007) Utility of imaging mass spectrometry (IMS) by matrix-assisted laser desorption ionization (MALDI) on an ion trap mass spectrometer in the analysis of drugs and metabolites in biological tissues. J Pharmacol Toxicol Methods 55(3):279–288
6. Shimma S, Sugiura Y, Hayasaka T, Hoshikawa Y, Noda T, Setou M (2007) MALDI-based imaging mass spectrometry revealed abnormal distribution of phospholipids in colon cancer liver metastasis. J Chromatogr 855(1):98–103
7. Stoeckli M, Chaurand P, Hallahan DE, Caprioli RM (2001) Imaging mass spectrometry: a new technology for the analysis of protein expression in mammalian tissues. Nat Med 7(4):493–496
8. Setou M, Heeren RM, Stoeckli M, Simma S, Matsumoto M (2007) Mass microscopy. Seikagaku 79(9):874–879
9. Rubakhin SS, Churchill JD, Greenough WT, Sweedler JV (2006) Profiling signaling peptides in single mammalian cells using mass spectrometry. Anal Chem 78(20):7267–7272
10. Luxembourg SL, Mize TH, McDonnell LA, Heeren RM (2004) High-spatial resolution mass spectrometric imaging of peptide and protein distributions on a surface. Anal Chem 76(18):5339–5344
11. Cooks RG, Ouyang Z, Takats Z, Wiseman JM (2006) Detection technologies. Ambient mass spectrometry. Science (New York, NY) 311(5767):1566–1570
12. Sugiura Y, Shimma S, Setou M (2006) Two-step matrix application technique to improve ionization efficiency for matrix-assisted laser desorption/ionization in imaging mass spectrometry. Anal Chem 78(24):8227–8235
13. Shimma S, Sugiura Y, Hayasaka T, Zaima N, Matsumoto M, Setou M (2008) Mass imaging and identification of biomolecules with MALDI-QIT-TOF-based system. Anal Chem 80 (3):878–885
14. Landgraf RR, Garrett TJ, Calcutt NA, Stacpoole PW, Yost RA (2007) MALDI-linear ion trap microprobe MS/MS studies of the effects of dichloroacetate on lipid content of nerve tissue. Anal Chem 79(21):8170–8175
15. Shimma S, Furuta M, Ichimura K, Yoshida Y, Setou M (2006) A novel approach to in situ proteome analysis using a chemical inkjet printing technology and MALDI-QIT-TOF tandem mass spectrometer. J Mass Spectrom Soc Japan 54:133–140
16. Groseclose MR, Andersson M, Hardesty WM, Caprioli RM (2007) Identification of proteins directly from tissue: in situ tryptic digestions coupled with imaging mass spectrometry. J Mass Spectrom 42(2):254–262
17. Walch A, Rauser S, Deininger SO, Hofler H (2008) MALDI imaging mass spectrometry for direct tissue analysis: a new frontier for molecular histology. Histochem Cell Biol 130(3):421–434

18. Caprioli RM, Farmer TB, Gile J (1997) Molecular imaging of biological samples: localization of peptides and proteins using MALDI-TOF MS. Anal Chem 69(23):4751–4760
19. Morita Y, Ikegami K, Goto-Inoue N, Hayasaka T, Zaima N, Tanaka H, Uehara T, Setoguchi T, Sakaguchi T, Igarashi H, Sugimura H, Setou M, Konno H (2009) Imaging mass spectrometry of gastric carcinoma in formalin-fixed paraffin-embedded tissue microarray. Cancer Sci 101(1):267–273
20. Ushijima M, Miyata S, Eguchi S, Kawakita M, Yoshimoto M, Iwase T, Akiyama F, Sakamoto G, Nagasaki K, Miki Y, Noda T, Hoshikawa Y, Matsuura M (2007) Common peak approach using mass spectrometry data sets for predicting the effects of anticancer drugs on breast cancer. Cancer Inform 3:285–293
21. Gahrton G (1964) Microspectrophotometric quantitation of the periodic acid-Schiff (PAS) reaction in human neutrophil leukocytes based on a model system of glycogen microdroplets. Exp Cell Res 34:488–506
22. Holness CL, Simmons DL (1993) Molecular cloning of CD68, a human macrophage marker related to lysosomal glycoproteins. Blood 81(6):1607–1613
23. Hayasaka T, Goto-Inoue N, Ushijima M, Yao I, Yuba-Kubo A, Wakui M, Kajihara S, Matsuura M, Setou M (2011) Development of imaging mass spectrometry (IMS) dataset extractor software, IMS convolution. Anal Bioanal Chem 401:183–193
24. Domon B, Costello CE (1988) Structure elucidation of glycosphingolipids and gangliosides using high-performance tandem mass spectrometry. Biochemistry 27(5):1534–1543

Loss of lymphatic vessels and regional lipid accumulation is associated with great saphenous vein incompetence

Hiroki Tanaka, MD,[a,b,c] Nobuhiro Zaima, PhD,[b,d] Takeshi Sasaki, PhD,[c] Naoto Yamamoto, MD,[a,c] Masaki Sano, MD,[a,c] Hiroyuki Konno, MD,[c] Mitsutoshi Setou, MD,[b] and Naoki Unno, MD,[a,c] *Hamamatsu and Nara, Japan*

Objective: Recent studies suggest that biologic changes in the vein wall associated with varicose veins (VVs) occur not only in valvular tissue but also in nonvalvular regions. We previously used imaging mass spectrometry (IMS) to determine the distribution of lipid molecules in incompetent valve tissue. In this study, we used IMS to analyze incompetent great saphenous veins (GSVs) in patients with varicose vein (VV) to assess the distribution of lipid molecules.

Methods: We obtained GSV tissue from 38 VV patients (50 limbs) who underwent GSV stripping. For the control veins (CV), we obtained GSV samples from 10 patients undergoing infrainguinal bypass with reversed GSV grafting for peripheral artery occlusive disease (10 limbs). Conventional and immunofluorescence staining were performed for histopathologic examination. The total lipid content in the homogenized vein tissue was determined. The localization of each lipid molecule in the vein wall was assessed by IMS.

Results: The histologic examination showed the VV walls were significantly thicker than the CV walls, and only the VV adventitia was positive for lipid staining. The VV wall had higher concentrations of phospholipids and triglycerides than the CV wall. IMS revealed an abnormal accumulation of lysophosphatidylcholine (LPC; 1-acyl 16:0) and phosphatidylcholine (diacyl 16:0/20:4) in the VV intima and media. Triglyceride was found only in VV adventitia. The number of lymphatic vessels, as measured by staining with D2-40, a lymphatic vessel-specific marker, was significantly lower in the VV adventitia than in the CV adventitia. Lymphatic vessel reduction may be associated with insufficient lymphatic drainage in the VV adventitia causing histologic changes in VV tissue.

Conclusions: The accumulation of LPC (1-acyl 16:0) and PC (diacyl 16:0/20:4) in the VV intima and media may be associated with chronic inflammation, leading to VV tissue degeneration. Furthermore, insufficient lipid drainage by lymphatic vessel may be responsible for accumulation of lipid molecules and subsequent vein wall degeneration. (J Vasc Surg 2012;55:1440-8.)

Clinical Relevance: Abnormal distribution of lipid molecules in varicose vein (VV) tissue in patients at CEAP class C_{2-3} and C_{4-5} suggests that VV-associated accumulation of lipid molecules begins in the early clinical stages of the disease and continues through the advanced stages. In particular, the accumulation of both lysophosphatidylcholine (1-acyl 16:0) and phosphatidylcholine (diacyl 16:0/20:4) in the media was significantly higher in VV tissue from patients in advanced clinical stages, suggesting an association between lipid accumulation and chronic inflammation of skin and subcutaneous tissues. Further study is needed to clarify the effect of lymph stasis on VVs and chronic inflammation. The mechanism whereby adventitial lymphatic vessels are damaged is also unknown. Consistent venous hypertension and subsequent overload to the lymphatics may account for the lymphatic damage. In addition, accumulation of possible proinflammatory lipid molecules in VV walls may further damage the adventitial lymphatic vessels.

We previously determined the characteristic distribution of lipid molecules in regions surrounding incompetent valves in patients with varicose veins (VVs) by using imaging mass spectrometry (IMS).[1] IMS revealed the accumulation of lysophosphatidylcholine (LPC; 1-acyl 16:0) and phosphatidylcholine (PC; diacyl 16:0/20:4) in the valvular region. Because these molecules are potential proinflammatory lipids,[2-4] this finding suggests that LPC and PC are involved in the development of tissue inflammation and valvular incompetence. These results support previously reported data.[5,6] However, recent studies suggest that histologic changes in the wall of the great saphenous vein (GSV) may precede valvular dysfunction.[5] The pathogenesis of these biologic changes is yet to be elucidated. Investigation of the lipid profile of the GSV wall may help gain insight into the influence of dyslipidemia in the VV tissues. For this purpose, we used IMS to analyze the

From the Division of Vascular Surgery,[a] the Department of Cell Biology and Anatomy Systems Molecular Anatomy,[b] the Second Department of Surgery,[c] and the Department of Anatomy,[c] Hamamatsu University School of Medicine, Hamamatsu; and the Department of Applied Biological Chemistry, Kinki University, Nara.[d]

This study was supported by Grant-in-Aid for Scientific Research (C) from the Japan Society for the Promotion of Science (NU).

Author conflict of interest: none.

Presented at the Twenty-third Annual Meeting of the American Venous Forum, San Diego, Calif, February 23-26, 2011.

Reprint requests: Naoki Unno, Division of Vascular Surgery, Hamamatsu University School of Medicine, 1-20-1 Handayama, Higashi-ku, Hamamatsu 431-192, Japan. (e-mail: unno@hama-med.ac.jp).

The editors and reviewers of this article have no relevant financial relationships to disclose per the JVS policy that requires reviewers to decline review of any manuscript for which they may have a competition of interest.

0741-5214/$36.00

doi:10.1016/j.jvs.2011.09.064